Processing and Application of Ceramics 14 [3] (2020) 268–275
https://doi.org/10.2298/PAC2003268Z

BY-NC-ND

Effect of $Al(OH)_3$ particle size on microstructures and strengths of porous $MgAl_2O_4$ ceramics

Jinna Zhi[1], Zhe Chen[1,*], Wen Yan[1,*], Stefan Schafföner[2], Yajie Dai[1], Xiaoli Lin[1]

[1]*The State Key Laboratory of Refractories and Metallurgy, Wuhan University of Science and Technology, Wuhan 430081, China*
[2]*Department of Materials Science and Engineering and Institute of Materials Science, University of Connecticut, Storrs, CT 06269, USA*

Received 23 December 2019; Received in revised form 12 May 2020; Received in revised form 16 July 2020; Accepted 5 August 2020

Abstract

Porous $MgAl_2O_4$ ceramics were prepared via in-situ decomposition pore-forming (ISDP) technique using $Al(OH)_3$ and magnesite as raw materials. The influence of $Al(OH)_3$ particle size (0–44 μm, 44–88 μm, 88–100 μm, 100–150 μm) on the microstructures and strengths of porous spinel ceramics were investigated by means of X-ray diffraction (XRD), scanning electron microscopy (SEM) and energy dispersive spectrometer (EDS). The bimodal distributions were observed among all the pore size distributions of the porous spinel ceramics. The small pores existed inside the particles and the big pores existed between the particles. When the $Al(OH)_3$ particle size decreased from 100–150 μm to 0–44 μm, the peak of large pores shifted towards left while intensity of the peak of small pores decreased. Simultaneously, the neck-bonds formed between particles grew significantly, which resulted in the increase of compressive strength from 1.4 to 10.8 MPa. The optimized product is the sample with the $Al(OH)_3$ particle size of 0–44 μm, which has a high apparent porosity (55.2%), a high compressive strength (10.8 MPa) and a relatively homogeneous pore size distribution.

Keywords: *porous $MgAl_2O_4$ ceramics, in-situ decomposition pore-forming technique, $Al(OH)_3$ particle size, microstructures, strengths*

I. Introduction

Spinel containing refractories are widely used as working linings of high-temperature furnaces, e.g. periclase-spinel refractories for cement rotary kilns and corundum-spinel refractories for steel ladles [1–7]. However, with the development of society, the pressure of energy conservation and emission reduction in high-temperature industry has increased. For industries involving high-temperature furnaces, such as steel or cement plants, in order to achieve green manufacturing, it is necessary to develop energy-saving thermal equipment by using high-efficiency energy-saving refractory as working linings, which can effectively reduce the energy consumption of steel and cement production processes [8–13]. Using porous spinel aggregates as raw materials is a good way to prepare high-efficiency and energy-saving spinel containing refractory lining [14–18]. These porous spinel aggregates could be obtained by crushing the porous spinel ceramics [19,20].

At present, the main preparation methods of porous spinel ceramics include foam-gelcasting route [21–26], template method [27–29], *in-situ* decomposition pore-forming (ISDP) technique [20,30–34], etc. For instance, Deng *et al.* [35] prepared the porous spinel foam ceramics with average pore size of 124–266 μm via foam-gelcasting route using spinel powders, but the pore sizes of these porous spinel ceramics were large and the pore distributions were inhomogeneous. Hashimoto *et al*. [28] fabricated porous spinel ceramics with an apparent porosity of 61.0% using porous alumina template and magnesium nitrate solution, but the preparation process was complicated and costs of raw materials were high.

* Corresponding author: tel: +86 027 68862511,
e-mail: *chenzhe2019@wust.edu.cn* (Z. Chen)
yanwen@wust.edu.cn (W. Yan)

Compared with foam-gelcasting route and template method, the *in-situ* decomposition pore-forming (ISDP) technique, which utilizes the decomposition of raw material to form pores, is a simple preparation process and environment-friendly way to prepare porous ceramics with well-distributed pores [33]. For example, Yan *et al*. [34] prepared porous spinel ceramics with a homogeneous pore size distribution using bauxite and magnesite as raw materials by ISDP technique to form pores. However, the contents of impurities in bauxite were high, which would affect the high-temperature properties of porous spinel ceramics. Porous spinel ceramics were prepared via the ISDP technique using aluminium hydroxide ($Al(OH)_3$) and basic magnesium carbonate [27] and hydrotalcite ($Mg_6Al_2(CO_3)(OH)_{16} \cdot 4\,H_2O$) [32], but the resulting strengths were too low.

To improve the strength of porous spinel ceramics, Yan *et al.* [33] manufactured the porous spinel ceramics with an apparent porosity of 42.1–44.2% and compressive strength of 51.1–52.0 MPa by employing magnesite and $Al(OH)_3$. However, the required high firing temperature (1780 °C) resulted in high energy consumption. Further, in order to reduce the firing temperature, 1.5 wt.% of TiO_2 additive was put into the mixtures of magnesite and $Al(OH)_3$ to promote the reaction sintering, and the porous spinel ceramics with an apparent porosity of 53.0% and strength of 21.2 MPa were fabricated after firing at 1600 °C [20]. Although the liquid phase formed by TiO_2 additive promoted the sintering process, the liquid phase also deteriorated their performances at high temperature. It was noted that the compressive strength of the samples without TiO_2 addition was only 3.9 MPa.

In addition to the increased firing temperature or introducing additives, the reduced particle size also plays a significant role in promoting sintering process, and further affects microstructure and strength of porous spinel ($MgAl_2O_4$) ceramics [36]. Therefore, in the present work, four porous $MgAl_2O_4$ ceramics were manufactured via ISDP using $Al(OH)_3$ powders with different particle size and magnesite powder as the raw materials, with the aim to improve the strength of porous spinel ceramics at lower firing temperature (1600 °C) without introducing any additives. Additionally, the effect of $Al(OH)_3$ particle size on the microstructure and properties of porous spinel ceramics was investigated.

II. Experimental procedure

Magnesite powder with the average particle size of 15.06 μm (Tongda Refractory Technologies Co, Ltd, China) and $Al(OH)_3$ powder with the average particle size of 88.90 μm (Aluminum Corporation of China Limited, China), having chemical compositions listed in Table 1, were used as raw materials. The $Al(OH)_3$ powder was ground with a ball mill and then sieved through different meshes to form four different powders with a particle size of 0–44 μm, 44–88 μm, 88–100 μm and 100–150 μm. Four porous spinel ceramics were prepared according to the formulation of raw materials listed in Table 2. The above starting powder mixtures were initially homogenised for 2 h in polyurethane pots with alumina balls and then pressed into cylinders (36 mm in height and 36 mm in diameter) under a pressure of 100 MPa. The green compacts were dried at 110 °C for 24 h and then heated at 1600 °C for 3 h in an electric furnace. In addition, in order to study the reaction process of magnesite and $Al(OH)_3$, the green compacts dried at 110 °C were also heated at 1400 °C for 3 h.

The phase compositions of the fired samples were characterized by X-ray diffraction (XRD, Philips Xperts TMP) with Cu K_α radiation (λ = 1.54187 Å) in 2θ range of 10–90° and a scanning speed of 2°/min. The apparent porosities and bulk densities of the fired samples were obtained by the Archimedes' principle using water as the immersion medium. The microstructures and element distributions were observed by field emission scanning electron microscope (FESEM, Nova 400 NanoSEM, FEI company, USA) equipped with energy dispersive X-ray spectroscope (EDS, INCA IE 350 pentaFET X-3, Oxford, UK). The pore size distributions were obtained by an image analysis method [22,37,38]. The compressive strengths at room temperature were measured according to the Chinese national standard GB/T 3997.2-1998.

Table 1. Chemical compositions of raw materials (wt.%)

	SiO_2	Al_2O_3	Fe_2O_3	CaO	MgO	K_2O	Na_2O	IL
$Al(OH)_3$	0.08	66.07	0.01	0.05	0.01	0.04	0.01	33.37
Magnesite	0.54	0.27	0.44	0.99	46.35	0.01	0	51.21

Table 2. Experimental formulations (wt.%)

Sample	Magnesite	$Al(OH)_3$			
		0–44 μm	44–88 μm	88–100 μm	100–150 μm
$S_{100\text{-}150}$	35	-	-	-	65
$S_{88\text{-}100}$	35	-	-	65	-
$S_{44\text{-}88}$	35	-	65	-	-
$S_{0\text{-}44}$	35	65	-	-	-

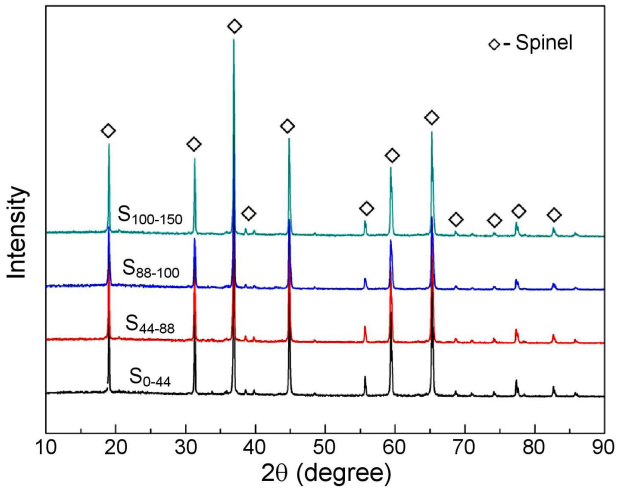

Figure 1. XRD patterns of the fired samples

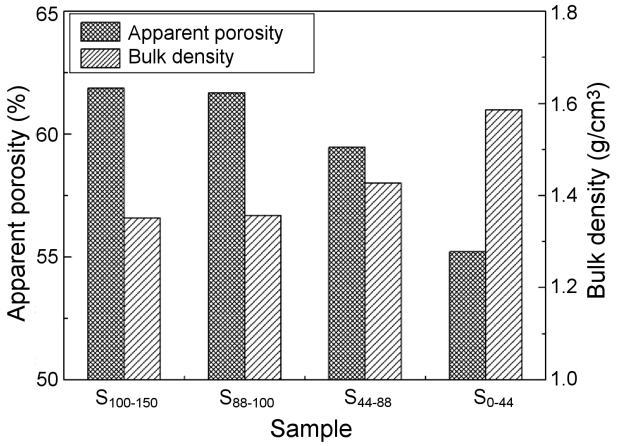

Figure 2. Apparent porosities and bulk densities of the fired samples

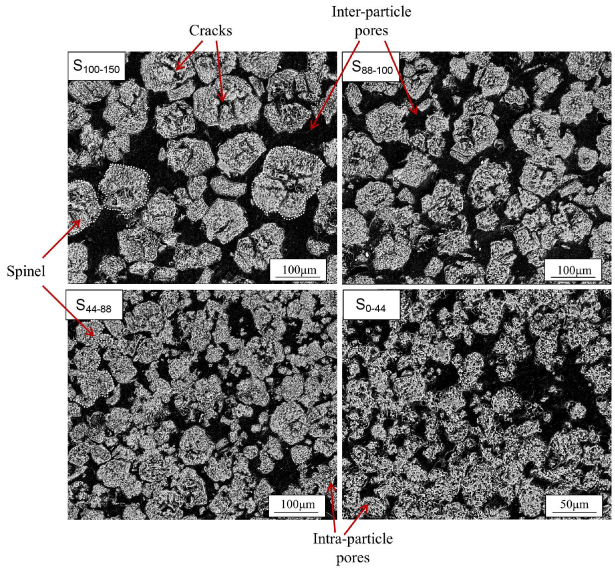

Figure 3. Microstructures of the fired samples

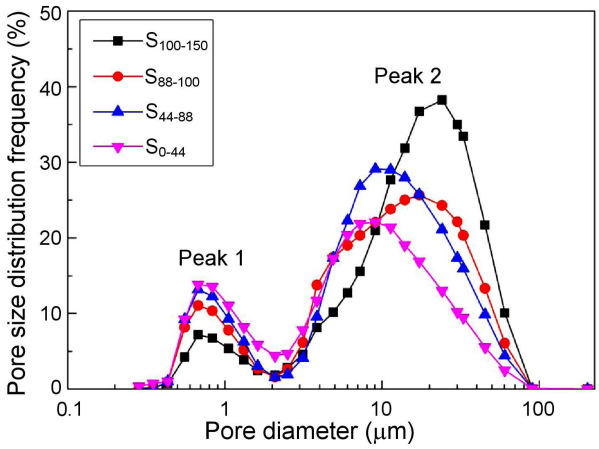

Figure 4. Pore size distributions of the fired samples

III. Results

The XRD patterns of the samples fired at 1600 °C are presented in Fig. 1. As it can be seen, no corundum or periclase were detected but only spinel phase was present which indicates that the raw materials have reacted completely to form spinel after the firing process.

The apparent porosities and bulk densities of the fired samples are given in Fig. 2. It is shown that with the decrease of $Al(OH)_3$ particle size, the apparent porosities decreased from 61.9% to 55.2%, and the bulk densities increased from 1.35 to 1.59 g/cm^3.

The microstructures of the fired samples are given in Fig. 3. SEM and EDS analyses supported the results of XRD confirming that only spinel phase was found in the fired samples. In SEM images, the black and light areas represent pores and spinel phase, respectively. Evidently, all the samples consisted of spinel particles and pores. The small pores located inside the particles are referred to as intra-particle pores, which originated from the decompositions of $Al(OH)_3$ and magnesite. The big pores referred to as inter-particle pores are located between the spinel particles, which originated from the packing behaviour of the mixed powders. In the sample $S_{100\text{-}150}$, the size of porous spinel particles and inter-particle pores are large. Besides, in this two-dimensional picture, the porous spinel particles are distributed in isolation, and there is no obvious neck connection between them. With the decrease of $Al(OH)_3$ precursor particle size, the particle size and distance between the porous spinel particles in the fired samples decrease obviously, forming a large number of neck connections between them.

In order to study the inter-particle pores and intra-particle pores characteristics, the pore size distributions of the fired samples are shown in Fig. 4. Bimodal distributions were observed among all the samples. For the inter-particle pores (Peak 2), with the decrease of $Al(OH)_3$ precursor particle size, the peak intensity decreases and curves shift towards the left, suggesting that the inter-particle pore area fraction was reduced. For the intra-particle pores (Peak 1), the intensity of the peak rises with the decrease of $Al(OH)_3$ particle size. In ad-

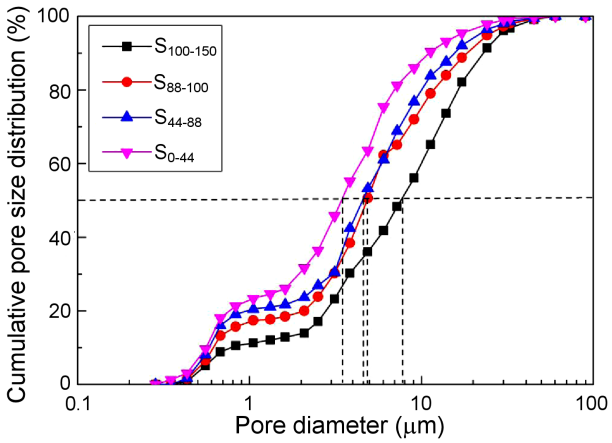

Figure 5. Cumulative pore size distributions of the fired samples

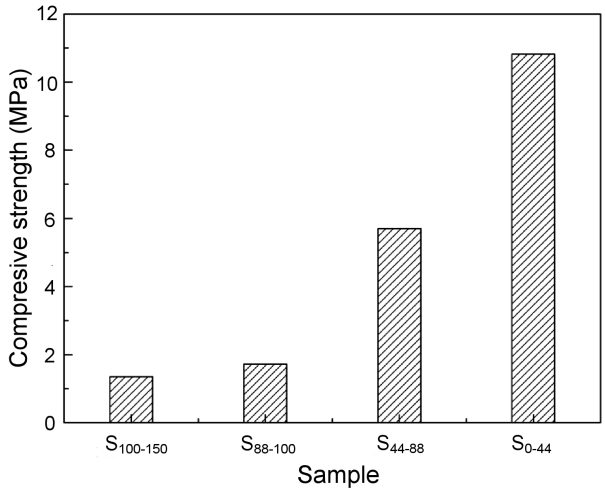

Figure 6. Compressive strengths of the fired samples

dition, the curves of cumulative pore size distributions are shown in Fig. 5. With decreasing $Al(OH)_3$ precursor particle size from 100–150 μm to 0–44 μm, the curves shift markedly towards left and the medium pore size declined from 7.9 to 3.4 μm.

The compressive strengths of the fired samples are given in Fig. 6. As the $Al(OH)_3$ particle size was 100–150 μm (the sample $S_{100\text{-}150}$), the compressive strength was only 1.4 MPa. When the decrease of $Al(OH)_3$ precursor particle size from 100–150 μm to 0–44 μm was detected, the compressive strength increased from 1.4 to 10.8 MPa.

IV. Discussion

Based on the above results, it can be seen that the reduced $Al(OH)_3$ precursor particle size can significantly promote the reaction-sintering process, reduce the pore size and effectively improve the strength of porous spinel ceramics. The apparent porosities, bulk densities and pore structure parameters of the samples prepared via the ISDP technique may be affected by four factors: i) the densities of green compacts, ii) the decompositions of $Al(OH)_3$ and magnesite, iii) the volume expansion derived from the formation of spinel and iv) the sintering reaction.

Firstly, the packing densities of green compacts had a great influence on the apparent porosities and pore sizes of samples. The particle size discrepancy between the $Al(OH)_3$ and magnesite particles is not considerable in the green compact $S_{0\text{-}44}$, while the $Al(OH)_3$ particle size in the other three samples is larger than the magnesite particle size. According to the packing behaviour of bimodal powder mixtures [36], the packing behaviour of particles in the green compact $S_{0\text{-}44}$ is consistent with the situation presented in Fig. 7a, while the packing behaviour of particles in the green compacts $S_{44\text{-}88}$, $S_{88\text{-}100}$ and $S_{100\text{-}150}$ changes from 7b to 7c. Therefore, the green compact $S_{0\text{-}44}$ has a lower packing density compared with the green compacts $S_{100\text{-}150}$, $S_{88\text{-}100}$ and $S_{44\text{-}88}$. The porosity of the green compacts increases with the decrease in the particle size of the $Al(OH)_3$ precursor powder (i.e. from $S_{100\text{-}150}$ to $S_{0\text{-}44}$) due to the decline of their packing density. As a result, the green compact $S_{0\text{-}44}$ has higher apparent porosity, but smaller average pore size compared with the samples $S_{100\text{-}150}$, $S_{88\text{-}100}$ and $S_{44\text{-}88}$.

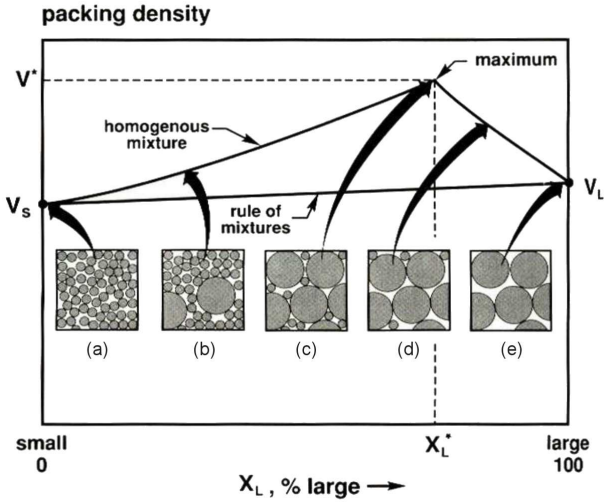

Figure 7. Relationship of the packing density with grain composition [36]

Secondly, the apparent porosities and pore sizes of samples were affected by the decompositions of $Al(OH)_3$ and magnesite particles. As it is well known, the $Al(OH)_3$ and magnesite particles decompose at about 300 °C and 670 °C, respectively [19]. After the decomposition of $Al(OH)_3$ and magnesite particles, porous agglomerations containing micro- and nanopores are formed, which we call pseudomorphs. In this work, the $Al(OH)_3$ and magnesite particles are decomposed completely at 1600 °C and the microstructures of the pseudomorphs are destroyed. In order to investigate the reaction process between $Al(OH)_3$ and magnesite pseudomorphs, the samples were fired at 1400 °C and their microstructures are shown in Fig. 8. It can be seen that the sizes of cracks caused by the decomposition of magnesite particles are small. However, the cracks

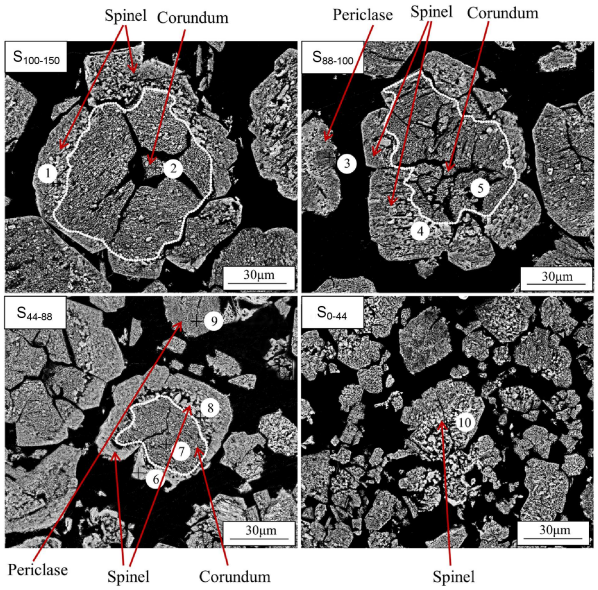

Figure 8. Microstructures of the samples fired at 1400 °C

caused by the decomposition of $Al(OH)_3$ particles look like petals with large sizes. It is clear that the size of petaloid cracks declines with the decrease of $Al(OH)_3$ precursor particle size, and then the porosity and pore size of samples are also reduced. Consequently, the fired sample $S_{0\text{-}44}$ with the smallest $Al(OH)_3$ particle size has lower apparent porosity and a smaller pore size than that of the $S_{100\text{-}150}$, $S_{88\text{-}100}$ and $S_{44\text{-}88}$.

Thirdly, the apparent porosities and pore sizes of samples were also affected by the volume expansion derived from the formation of spinel. To investigate the formation process of spinel in the samples containing $Al(OH)_3$ and magnesite pseudomorphs, EDS analyses were performed. It is illustrated in Fig. 8 and Table 3 that if the size of $Al(OH)_3$ particles is smaller, the pseudomorph with lower content and smaller size of corundum phase was formed in the samples fired at 1400 °C (points 2, 5 and 7). When the particle size is small, $Al(OH)_3$ can easily react with magnesite completely. This causes the reduction in size of the magnesite pseudomorph (points 3 and 9) and increase of the thickness of the formed spinel rings (points 1, 4, 8 and 10). It was clear that the amount of $Al(OH)_3$ pseudomorphs increased with the decrease of $Al(OH)_3$ precursor particle size, which resulted in a higher probability of reaction with magnesite pseudomorphs to form spinel. Therefore, the spinel formation from $Al(OH)_3$ pseudomorphs is easier in the sample $S_{0\text{-}44}$ with the smallest $Al(OH)_3$ precursor particle size relatively to other samples. As it is well known, about 8% volume expansion will occur in the spinel formation process [22,39]. Thus, the volume expansion of spinel can fill the pores between particles and then reduce the apparent porosities and pore sizes of a sample. Because of that the sample $S_{0\text{-}44}$ with the smallest $Al(OH)_3$ precursor particle size has low apparent porosity and relatively small pore size.

Finally, the sintering reaction was another important factor influencing the apparent porosities and pore sizes of the samples. With the decrease of $Al(OH)_3$ particle size, the sintering reaction between particles is promoted. When the $Al(OH)_3$ particle size is small, the number of neck bonds between particles is large and the sintering densification degree of samples is relatively high. Thus, the fired sample $S_{0\text{-}44}$ prepared from the $Al(OH)_3$ with the smallest particle size has low apparent porosity and the smallest pore size.

It is well known that microstructure affects strength of porous spinel ceramics strongly. Thus, the decrease of $Al(OH)_3$ precursor particle size can promote the neck bonding between particles and densification degree, which result in a higher strength of porous spinel ceramics.

The pore formation mechanism of porous spinel ceramics can be put forward from the above results, as it is shown in Fig. 9. At the initial stage after mixing and pressing, the model of contacting between $Al(OH)_3$ and magnesite particles is above 670 °C, $Al(OH)_3$ and magnesite decompose thoroughly and generate $Al(OH)_3$ and magnesite pseudomorphs with a large number of micropores (Fig. 9b). The distribution of cracks in magnesite pseudomorphs is homogeneous, while the cracks existing in $Al(OH)_3$ pseudomorphs are petaloid like. The petaloid cracks extend from the centre to the edge of particles, as presented in Fig. 9c. With the further increase of firing temperature, particle arrangement

Table 3. EDS analysis of points presented in Fig. 8 (at.%)

Point	O	Mg	Al	Ca	Possible phases
1	56.41	13.45	30.14		spinel
2	54.35		45.65		corundum
3	39.93	60.07			periclase
4	50.53	15.67	33.80		spinel
5	41.28		56.60		corundum
6	50.91	13.43	34.42	1.42	spinel, glass phase
7	58.39		41.61		corundum
8	48.78	14.88	36.34		spinel
9	38.07	61.93			periclase
10	47.59	16.21	36.20		spinel

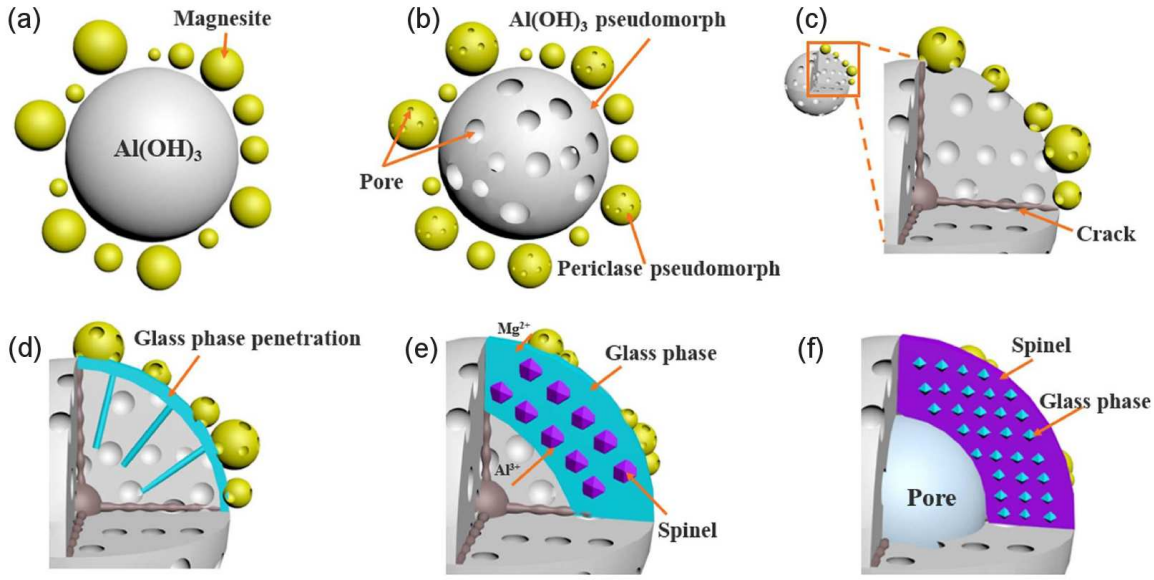

Figure 9. Pore forming mechanism of porous spinel ceramics: a) initial state , b) decomposition of raw material, c) an enlarged region depicting the internal structure of $Al(OH)_3$, d) penetration of liquid, e) spinel precipitation and particle rearrangement and f) particles densification

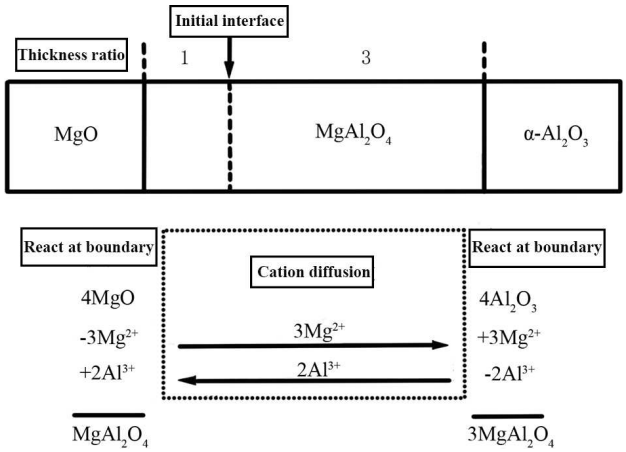

Figure 10. Forming mechanism of $MgAl_2O_4$ [40]

occurs and low melting point phases are generated from the impurities. The inter-diffusion rate of Mg^{2+} and Al^{3+} rise, then spinel phases are formed and result in volume expansion, as shown in Figs. 9d and 9e. According to electricity balance, shown in Fig. 10, 3 mol Mg^{2+} diffuse towards the $Al(OH)_3$ pseudomorph and produce 3 mol of spinel. Meanwhile, 2 mol of Al^{3+} spread towards the magnesite pseudomorph and produce 1 mol of spinel. Consequently, the cyclic spinel is easier to be generated around the $Al(OH)_3$ pseudomorph [19]. After the reaction of raw materials is completely finished, the particles become relatively dense and cyclic spinel containing central pores are formed as illustrated in Fig. 9f.

It should be pointed out that as it can be seen in our another similar study [20], when 0 wt.% of TiO_2 additive was added into the mixtures of magnesite and $Al(OH)_3$, the porous spinel ceramics with a compressive strength of 3.9 MPa was fabricated after firing at 1600 °C. Compared with these results [20], in the present work we have prepared porous spinel ceramics with a significantly higher compressive strength of 10.8 MPa after firing at 1600 °C by reducing the particle size of $Al(OH)_3$. Therefore, it is feasible to prepare porous spinel ceramics with a higher strength by reducing particle size of $Al(OH)_3$ precursor powder.

V. Conclusions

Porous $MgAl_2O_4$ ceramics with high porosities and high strengths have been prepared using $Al(OH)_3$ powders with different particle size and magnesite powder as raw materials by *in-situ* decomposition pore-forming (ISDP) technique. $Al(OH)_3$ particle size strongly affects porosities, pore size distributions and strengths of the fired samples. The following conclusions can be reached:

(1) In all the samples, the bimodal distributions of pore size were observed. As the $Al(OH)_3$ particle size changed from 100–150 μm to 0–44 μm, the peak of big pores shifted towards the left while the peak values of small pores decreased.

(2) With the decrease of $Al(OH)_3$ particle size, the neck-bonds formed between particles were significantly developed, which led to the strengths of porous spinel ceramics increasing from 1.4 to 10.8 MPa.

(3) The optimized product is the sample with 0–44 μm $Al(OH)_3$ particle size, which had a high apparent porosity of 55.2%, a high compressive strength of 10.8 MPa and a relatively homogeneous pore size distribution.

Acknowledgements: The authors would like to thank the Project of the National Natural Science Foundation of China (Grant No. 51974214), the Key Project of the National Natural Science Foundation of China (Grant No. U1860205) and the Key Projects of Hubei Provin-

cial Department of Education's Scientific Research Plan of China (Grant No. D20181106) for financially supporting this work.

References

1. Y. Liang, A. Huang, X. Zhu, H. Gu, L. Fu, "Dynamic slag/refractory interaction of lightweight Al_2O_3-MgO castable for refining ladle", *Ceram. Int.*, **41** (2015) 8149–8154.
2. Y. Zou, H. Gu, A. Huang, M. Zhang, C. Ji, "Effects of MgO micropowder on microstructure and resistance coefficient of Al_2O_3-MgO castable matrix", *Ceram. Int.*, **40** (2014) 7023–7028.
3. N. Shinozaki, Y. Takahashi, K. Mukai, "Interfacial reaction between Al_2O_3-MgO substrates and liquid iron", *J. Jpn. Inst. Met.*, **59** (1995) 1018–1023.
4. S.M. Zubakov, G.V. Kononenko, "Wear of high-fired periclase-spinel refractories in the roof of a double-bath steel-melting furnace", *Refractories*, **14** [5-6] (1973) 295–299.
5. X. Lin, W. Yan, Q. Chen, N. Li, S. Ma, W. Zhou, "Effect of spinel content on the reaction of porous periclase-spinel ceramics and cement clinker", *Key Eng. Mater.*, **697** (2016) 581–585.
6. L. Fu, A. Huang, H. Gu, H. Ni, "Properties and microstructures of lightweight alumina containing different types of nano-alumina", *Ceram. Int.*, 44 [15] (2018) 17885–17894.
7. Z. Chen, W. Yan, S. Schafföner, S. Ma, Y. Dai, N. Li, "Effect of SiC powder content on lightweight corundum-magnesium aluminate spinel castables", *J. Alloys Compd.*, **764** (2018) 210–215.
8. C. Connors Sr., "Energy-saving refractories", *Ceram. Ind.*, **158** [3] (2008) 31.
9. W. Yan, G. Wu, S. Ma, S. Schafföner, Y. Dai, Z. Chen, "Energy efficient lightweight periclase-magnesium alumina spinel castables containing porous aggregates for the working lining of steel ladles", *J. Eur. Ceram. Soc.*, **38** [12] (2018) 4276–4282.
10. B.L. Krasnyi, V.P. Tarasovskii, A.B. Krasnyi, "Use of new ceramic and refractory materials-an important factor in improving the economic and energy efficiency of enterprises, and their ecological security", *Refract. Ind. Ceram.*, **51** [4] (2010) 236–246.
11. R. Yin, *Metallurgical Process Engineering*, Metallurgical Industry Press, Beijing and Springer-Verlag Berlin Heidelberg, 2011.
12. A. Huang , H. Gu , Z. Yang , L. Fu, P. Lian, L. Jin, "An approach for modeling slag corrosion of lightweight Al_2O_3-MgO castables in refining ladle", pp. 101–111 in *Advanced and Refractory Ceramics for Energy Conservation and Efficiency*. Eds. H.T. Lin and J. Hemrick. John Wiley & Sons, USA, 2016.
13. L. Fu, H. Gu, A Huang, M. Zhang, X. Hong, L. Jin, "Possible improvements of alumina-magnesia castable by lightweight microporous aggregates", *Ceram. Int.*, **41** [1] (2015) 1263–1270.
14. N. Xu, S. Li, Y. Li, Z. Xue, L. Yuan, J. Zhang, L. Wang, "Preparation and properties of porous ceramic aggregates using electrical insulators waste", *Ceram. Int.*, **41** [4] (2015) 5807–5811.
15. R. Chen, Y. Li, R. Xiang, S. Li, X. Fan, Y. Li, S. Sang, "Effect of pyrophyllite addition on properties of lightweight insulation refractory materials", *Chin. Refract.*, **26** [3] (2017) 38–42.
16. G. Wu, W. Yan, S. Schafföner, Y. Dai, B. Han, T. Li, S. Ma, N. Li, G. Li, "A comparative study on the microstructures and mechanical properties of a dense and a lightweight magnesia refractories", *J. Alloys Compd.*, **796** (2019) 131–137.
17. Z. Chen, W. Yan, Y. Dai, S. Schafföner, B. Han, N. Li, "Effect of microporous corundum aggregates on microstructure and mechanical properties of lightweight corundum refractories", *Ceram. Int.*, **45** [7] (2019) 8533–8538.
18. G. Wu, W. Yan, S. Schafföner, X. Lin, S. Ma, Y. Zhai, X. Liu, L. Xu, "Effect of magnesium aluminate spinel content of porous aggregates on cement clinker corrosion and adherence properties of lightweight periclase-spinel refractories", *Constr. Build. Mater.*, **185** (2018) 102–109.
19. X. Lin, W. Yan, N. Li, "Phase composition and pore evolution of porous periclase-spinel ceramics prepared from magnesite and $Al(OH)_3$", *Sci. Sinter.*, **48** [2] (2016) 147–155.
20. W. Yan, X. Lin, J. Chen, N. Li, Y. Wei, B. Han, "Effect of TiO_2 addition on microstructure and strength of porous spinel ($MgAl_2O_4$) ceramics prepared from magnesite and $Al(OH)_3$", *J. Alloys Compd.*, **618** (2015) 287–291.
21. H. Chen, F. Liang, W. Fang, H. Chen, X. Du, F. Wang, L. Zhao, "Fabrication of microporous corundum-spinel refractory castables by foam-gelcasting methods", *J. Mater. Eng. Perform.*, **24** [8] (2015) 3049–3055.
22. I. Ganesh, "Fabrication of magnesium aluminate ($MgAl_2O_4$) spinel foams", *Ceram. Int.*, **37** [7] (2011) 2237–2245.
23. L. Yuan, B. Ma, Q. Zhu, X. Zhang, H. Zhang, J. Yu, "Preparation and properties of mullite-bonded porous fibrous mullite ceramics by an epoxy resin gel-casting process", *Ceram. Int.*, **43** [7] (2017) 5478–5483.
24. W. Zhou, W. Yan, N. Li, Y. Li, Y. Dai, Z. Zhang, "Effect of microsilica content on microstructure and properties of foamed ceramics with needle-like mullite", *Process. Appl. Ceram.*, **13** [2] (2019) 202–209.
25. W. Zhou, W. Yan, N. Li, Y. Li, Y. Dai, Z. Zhang, "Fabrication of mullite-corundum foamed ceramics for thermal insulation and effect of micro-pore-foaming agent on their properties", *J. Alloys Compd.*, **785** (2019) 1030–1037.
26. W. Zhou, W. Yan, N. Li, Y. Li, Y. Dai, B. Han, Y. Wei, "Preparation and characterization of mullite foam ceramics with porous struts from white clay and industrial alumina", *Ceram. Int.*, **44** [18] (2018) 22950–22956.
27. R. Salomao, M.O.C.V. Bôas, V.C. Pandolfelli, "Porous alumina-spinel ceramics for high temperature applications", *Ceram. Int.*, **37** [4] (2011) 1393–1399.
28. S. Hashimoto, S. Honda, T. Hiramatsu, Y. Iwamoto, "Fabrication of porous spinel ($MgAl_2O_4$) from porous alumina using a template method", *Ceram. Int.*, **39** [2] (2013) 2077–2081.
29. K. Yan, X. Wu, X. An, X. Xie, "Facile synthesis and catalytic property of spinel ferrites by a template method", *J. Alloys Compd.*, **552** (2013) 405–408.
30. Q. Chen, W. Yan, N. Li, X. Lin, Z. Zhang, B. Han, Y. Wei, "Effect of $Al(OH)_3$ content on the microstructure and strength of porous cordierite-mullite ceramics prepared by an in-situ pore forming technique", *Sci. Sinter.*, **50** (2018) 205–215.
31. W. Yan, N. Li, B.Q. Han, "High-strength lightweight

spinel refractories", *Am. Ceram. Soc. Bull.*, **84** [4] (2005) 9201–9203
32. S. Li, N. Li, Y. Li, "Processing and microstructure characterization of porous corundum-spinel ceramics prepared by in situ decomposition pore-forming technique", *Ceram. Int.*, **34** [5] (2008) 1241–1246.
33. W. Yan, J. Chen, N. Li, W. Qiu, Y. Wei, B. Han, "Preparation and characterization of porous MgO-Al_2O_3 refractory aggregates using an in-situ decomposition pore-forming technique", *Ceram. Int.*, **41** [1] (2015) 515–520.
34. W. Yan, N. Li, Y. Li, G. Liu, B. Han, J. Xu, "Effect of particle size on microstructure and strength of porous spinel ceramics prepared by pore forming in situ technique", *Bull. Mater. Sci.*, **34** [5] (2011) 1109–1112.
35. X. Deng, J. Wang, J. Liu, H. Zhang, L. Han, S. Zhang, "Low cost foam-gelcasting preparation and characterization of porous magnesium aluminate spinel ($MgAl_2O_4$) ceramics", *Ceram. Int.*, **42** [16] (2016) 18215–18222.
36. R.M. German, *Sintering Theory and Practice*, Wiley-Interscience, 1996.
37. S. Ma, W. Yan, S. Schafföner, X. Lin, N. Li, Y. Zhai, X. Liu, L. Lin, "Influence of magnesium aluminate spinel powder content on cement clinker corrosion and adherence properties of lightweight periclase-spinel refractories", *Ceram. Int.*, **43** [18] (2017) 17026–17031.
38. Z. Zhang, W. Yan, N. Li, Y. Li, W. Zhou, B. Han, "Influence of spherical porous aggregate content on microstructures and properties of gas-permeable mullite-corundum refractories", *Ceram. Int.*, **45** [14] (2019) 17268–17275.
39. I. Ganesh, K.A Teja, N. Thiyagarajan, R. Johnsonet, "Formation and densification behavior of magnesium aluminate spinel: The influence of CaO and moisture in the precursors", *J. Am. Ceram. Soc.*, **88** [10] (2005) 2752–2761.
40. N. Li, H. Gu, H. Zhao, *Refractories Fundamental and Technology*, Metallurgical Industry Press, Beijing, 2010. (in Chinese).